

Eccentricity distribution of wide low-mass binaries

Andrei Tokovinin*

*Cerro Tololo Inter-American Observatory/ NSF's National Optical-Infrared Astronomical Research Laboratory
Casilla 603, La Serena, Chile*

ABSTRACT

Distribution of eccentricities of very wide (up to 10 kau) low-mass binaries in the solar neighborhood is studied using the catalogue of El-Badry and Rix (2018) based on *Gaia*. Direction and speed of relative motions in wide pairs contain statistical information on the eccentricity distribution, otherwise inaccessible owing to very long orbital periods. It is found that the eccentricity distribution is close to the linear (thermal) one $f(e) = 2e$. However, pairs with projected separations < 200 au have less eccentric orbits, while $f(e)$ for wide pairs with $s > 1$ kau appears to be slightly super-thermal, with an excess of very eccentric orbits. Eccentricity of any wide binary can be constrained statistically using direction and speed of its motion. The thermal eccentricity distribution signals an important role of the stellar dynamics in the formation of wide binaries, although disk-assisted capture also can produce such pairs with eccentric orbits.

Key words: binaries: visual

1 INTRODUCTION

Formation of binaries is an actively debated subject. It is already clear that multiple systems are formed by several different mechanisms and that binary statistics depend on the environment. However, quantitative and predictive models are still lacking.

Orbits of wide binaries are a fossil record of their formation process and early dynamical evolution. In this note, I focus on the eccentricity distribution. Dynamical interactions in a cluster are expected to produce a “thermal” eccentricity distribution $f(e) = 2e$, although this state might not be reached in actual clusters (Geller et al. 2019). Decay of chaotic triple stars leads to a slightly super-thermal eccentricity distribution (Stone & Leigh 2019), while eccentricities of binaries surviving interactions with other stars (scattering) are distributed thermally (Antognini & Thompson 2016). On the other hand, dissipative forces (tides or gas friction) tend to decrease the eccentricity. Ejections from unstable triples, on the contrary, produce wide binaries with very eccentric orbits and a “super-thermal” $f(e)$ (Reipurth & Mikkola 2012).

Here a catalogue of wide binaries within 200 pc compiled by El-Badry & Rix (2018, hereafter ER2018) on the basis of *Gaia* second data release (Gaia collaboration 2018) is used. Accurate astrometry allows measurement of relative motion in the nearby resolved pairs which, in turn, contains some information on the eccentricity. Tokovinin & Kiyaveva

(2016) explored this option using classical (pre-*Gaia*) data on binaries within 67 pc with separations from 50 to a few hundred au. The new *Gaia* sample of wide binaries is larger and more accurate, allowing us to reach the regime of very wide separations.

The method of Tokovinin & Kiyaveva (2016) is based on the statistics of two quantities: (i) the angle γ between the line joining binary components (radius vector) and the direction of their instantaneous orbital motion (vector of relative velocity), and (ii) the normalized orbital speed μ' . Both quantities refer to the plane of the sky (i.e. are projected) and can be measured for a wide binary from the position and motion of the secondary component relative to the primary.

The characteristic orbital speed μ^* (in angular units per year) is computed by the formula

$$\mu^* = (2\pi\rho)/P^* = 2\pi\rho^{-1/2}\varpi^{3/2}M^{1/2}, \quad (1)$$

where ρ is the separation between the components, P^* is the notional orbital period in years estimated for a face-on circular orbit from the projected separation $s = \rho/\varpi$, ϖ is the parallax, and M is the mass sum in solar units. If μ is the measured speed of the orbital motion, $\mu' = \mu/\mu^*$ is its normalized equivalent. A bound system must have $\mu' < \sqrt{2}$. The angle γ is folded in the $(0, 90^\circ)$ interval.

Simulations from Tokovinin & Kiyaveva (2016) show that for a thermal eccentricity distribution, γ is distributed uniformly and uncorrelated with μ' , while median $\mu' = 0.546$. If $f(e)$ is sub-thermal (i.e. the orbits are, on average, more circular), the median γ increases and becomes posi-

* E-mail: atokovinin@ctio.noao.edu

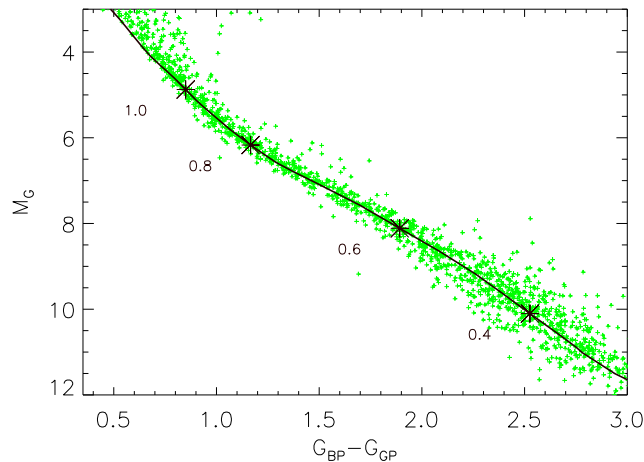


Figure 1. Color-magnitude diagram for the primary (brighter) components of wide binaries within 67 pc. The dark line is a 1-Gyr solar-metallicity isochrone (Bressan et al. 2012), where the asterisks and numbers mark masses.

tively correlated with μ' . The fingerprint of a super-thermal distribution is just the opposite.

Relevant characteristics of nearby wide binaries and the role of inner subsystems are covered in Section 2. The eccentricity distribution is addressed in Section 3, first qualitatively by examining the distributions of μ' and γ , then by inverting these distributions to derive $f(e)$. Statistical constraints on the eccentricity of any given wide binary that can be deduced from its motion are outlined. Section 4 discusses the results in the context of binary formation.

2 CHARACTERISTICS OF THE SAMPLE

2.1 Catalogue properties

The catalogue of ER2018 was recovered from the journal web site as a comma-separated text file. Only 3601 pairs of main-sequence stars with both parallaxes exceeding 15 mas are kept in our subset of the catalogue. The rationale for selecting only nearby pairs is the increased accuracy of the orbital speed measurement (particularly relevant for the widest pairs), better screening for subsystems, and access to low-mass, closer pairs. At larger distances, the ER2018 catalogue suffers from the increasing incompleteness.

Figure 1 shows the color-magnitude diagram (CMD) of the primary components in the *Gaia* colors. The 1-Gyr PARSEC isochrone (Bressan et al. 2012) traces the main sequence. Masses are estimated from this isochrone and absolute G magnitudes. Some stars with masses above $1 M_{\odot}$ are evolved. To avoid evolved systems, the statistical analysis below is restricted to primary masses less than $1 M_{\odot}$, rejecting about 20% of the more massive pairs. Most pairs have primary components of G, K, M spectral types, with a lowest mass of about $0.2 M_{\odot}$ and a median mass of $0.6 M_{\odot}$. Figure 18 of El-Badry & Rix (2018) shows a binary-star sequence in the CMD which is practically absent in the sample studied here. The likely reason is a better rejection of inner subsystems in the nearby wide pairs.

Most pairs have separations between 100 and a few

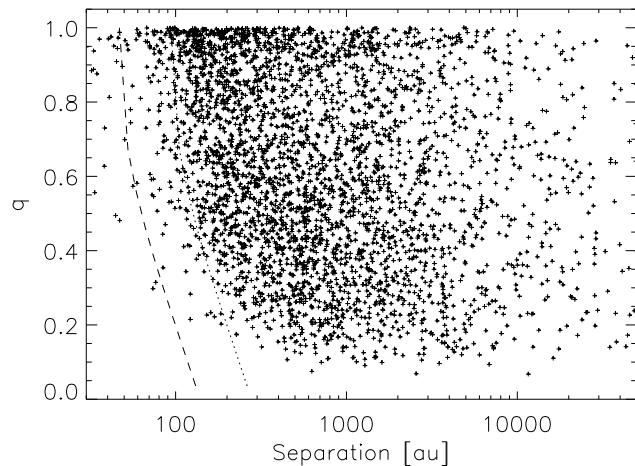


Figure 2. Correlation between separation and mass ratio. The dashed line is the *Gaia* detection limit at 67 pc, the dotted line is twice the limit.

thousand au; the median separation is 460 au, corresponding to an orbital period of ~ 10 kyr. The ER2018 catalogue has a minimum angular separation of $2''$ that translates to 133 au at 67 pc. Therefore, pairs with $s < 133$ au come from a smaller volume and their number is reduced substantially, preventing analysis of closer binaries. The maximum of the binary separation distribution at ~ 50 au or less (Raghavan et al. 2010) is not sampled by this catalogue. Consequently, I focus only on wide pairs.

Correlation between the mass ratio $q = M_2/M_1$ and the separation is illustrated in Fig. 2: pairs with larger q tend to be closer and, conversely, wide pairs seem to prefer smaller q . Please, refer to El-Badry et al. (2019) for a more detailed study of the mass-ratio dependence on primary mass and separation. The dashed line is the approximate binary detection limit in *Gaia*, $\Delta G < 5.5[(\rho/1'') - 0.7]^{0.4}$ at the maximum distance of 67 pc, converted into q by the relation $q \approx 1 - 0.16\Delta G$ valid for $M_1 \sim 0.6 M_{\odot}$ (see Fig. 8 of El-Badry et al. 2019). The dotted line is twice this separation. Figure 2 suggests that the criteria imposed in the creation of the ER2018 catalogue effectively remove pairs with separations less than ~ 2 times the detection limit.

2.2 Multiple systems

The ER2018 catalogue is not fully representative of the unbiased population of wide binaries for two main reasons. First, members of moving groups and clusters are excluded. Second, the selection method (good-quality astrometry and photometry, matching proper motions) creates a strong bias against subsystems. Remember that sub-arcsecond pairs often lack *Gaia* astrometry, hence have no chance to be present in the catalogue as components of wider pairs. When *Gaia* does provide astrometry of both stars, it can still be distorted by subsystems (large errors and/or biased PMs), eliminating wide pairs containing subsystems from the catalogue. However, many subsystems still remain.

The ER2018 catalogue was cross-identified with the 2018 version of the Washington Double Star (WDS) catalogue (Mason et al. 2001) to look for known subsystems around primary and secondary components. The resulting

list of 419 candidates was examined manually and compared to the Multiple Star Catalogue, MSC (Tokovinin 2018), version of July 2019. Most hierarchies were already present in the MSC, the missing ones were added. It is well known that WDS contains optical and spurious pairs, and the cross-list counts many such cases. Decision on the reality of each subsystem, if not obvious, is based on the available data and my experience, and in some cases can be questioned. Overall, I found that 166 pairs in the ER2018 catalogue within 67 pc contain known subsystems.

To further explore hidden multiplicity, I used the list of *Hipparcos* stars with astrometric accelerations by Brandt (2018) and matched stars within 67 pc with the WDS. Systems where the estimated period of the wide pair exceeds ~ 1000 yr are triple. Several hundred new triples were added to the MSC as a result of this effort. After this update, comparison of the MSC with the ER2018 catalogue within 67 pc reveals 226 multiples, i.e. 60 additional hierarchies detected by acceleration. The total fraction of known multiples in the catalogue is 0.063. In the following analysis, hierarchical systems (i.e. wide pairs with inner subsystems) present in the MSC are marked by a flag. Obviously, there remain many unknown subsystems, especially among fainter stars not covered by *Hipparcos* and Brandt (2018). El-Badry & Rix (2018) estimate that as much as 0.36 fraction of their sample could contain a subsystem in one or both components, despite the bias against multiples inherent to this catalogue. The fraction of undetected subsystems in the subset of nearby wide binaries studied here should be less than in the full catalogue.

3 ECCENTRICITY DISTRIBUTION

3.1 Qualitative view

Parameters of the relative motion of wide pairs are computed from the *Gaia* astrometry provided in the ER2018 catalogue. The modulus of the relative proper motion (PM) μ is computed from the PMs of each component, and its error is computed by eq. 6 in ER2018. The separation ρ and position angle θ of the pair are computed from the components' coordinates. The angle of the relative PM θ_μ is computed similarly. The angle γ is evaluated in three steps: $\gamma_1 = |\theta - \theta_\mu|$, $\gamma_2 = \gamma_1$ modulo 180° , $\gamma = \gamma_2$ for $\gamma_2 < 90^\circ$ and $\gamma = 90^\circ - \gamma_2$ otherwise. The error of γ is determined by the relative PM error, and expressed in degrees: $\sigma_\gamma = 57.3 \sigma_\mu / \mu$, based on the assumption that PM errors are isotropic. The characteristic PM μ^* is computed using (1). The calculation of μ' accounts for a small bias due to measurement errors: $\mu' = \sqrt{\mu^2 - \sigma_\mu^2} / \mu^*$. However, the results are similar if this correction is neglected.

The following statistics use wide pairs satisfying the following conditions:

- $M_1 < 1 M_\odot$
- $\sigma_\gamma < 50^\circ$
- $\mu' < 1.41$
- Not multiple

Filtering leaves 2663 pairs for further analysis. The large tolerance on σ_γ is intentional to avoid potential bias in the statistics caused by rejection of slowly moving pairs. Only

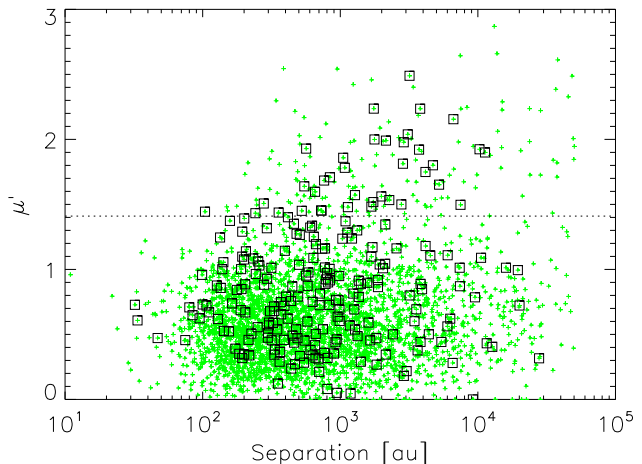


Figure 3. Statistics of “fast movers”: dependence of μ' on projected separation. Known multiples are marked by squares, the dotted line marks $\mu' = 1.41$.

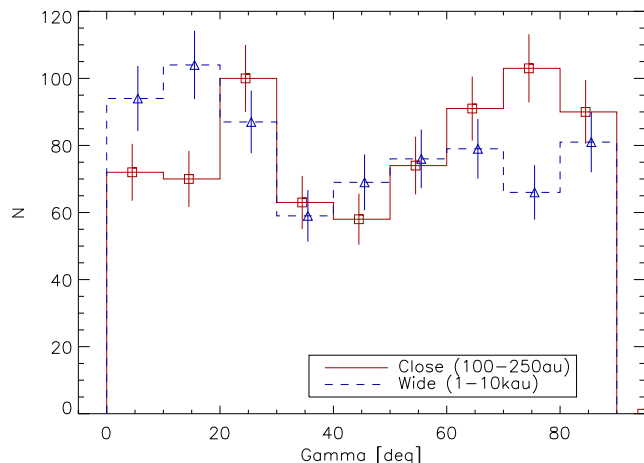


Figure 4. Histograms of γ for close ($100 < s < 250$ au, $N = 721$) and wide ($10^3 < s < 10^4$ au, $N = 715$) pairs.

99 (3.7%) of the 2663 accepted pairs have $20^\circ < \sigma_\gamma < 50^\circ$. Very similar results are obtained with the stricter $\sigma_\gamma < 20^\circ$ cut.

Apparently unbound pairs with $\mu' > 1.41$, or “fast movers”, deserve a closer look. Their total number is 179, or 0.05 fraction of all pairs. Reasons such as measurement errors or hidden multiplicity reveal themselves in the statistics of fast movers explored in Fig. 3. The widest (hence slower moving) pairs should be more affected by these factors. Indeed, the fraction of fast movers increases with separation: it is $86/1086=0.079$ for s between 10^3 and 10^4 au and $29/157=0.185$ for $s > 10^4$ au. On the other hand, the fraction of fast movers does not depend on the distance. This suggests that measurement errors are not the dominant factor and that fast movers are mostly caused by motions of inner subsystems. Indeed, the fraction of known multiples among the fast movers, $37/179=0.21$, is much larger than the fraction of multiples in the full catalogue, 0.06. Belokurov et al. (2020, Sect. 3.5) prove that excessive motion of some wide pairs in the ER2018 catalogue is related

Table 1. Medians of μ' and γ and correlation $C_{\mu'\gamma}$

Sample	N	γ_{med}	μ'_{med}	$C_{\mu'\gamma}$
(1) All	2663	44.7 \pm 1.0	0.542	-0.02
(2) 100–200 au	515	51.2 \pm 2.1	0.531	0.03
(3) 200–400 au	598	43.7 \pm 2.9	0.523	-0.09
(4) $10^3 - 10^4$ au	715	41.5 \pm 2.2	0.554	0.01
(5) Multiple	226	43.9 \pm 2.6	0.842	-0.06
$f(e) = 2e$	—	45.0	0.546	0.00
$f(e) = 1$	—	54.1	0.606	0.18
$e = 0$	—	68.3	0.677	0.61

to unresolved inner subsystems, rather than to a modified gravity law, as suggested by Pittordis & Sutherland (2019).

Table 1 gives the median values of γ and μ' and their correlation coefficient $C_{\mu'\gamma}$ for the full sample (1), subsamples (2)-(4) selected according projected physical to separation, and the control sample (5) of pairs with subsystems. The errors of the γ medians are estimated by bootstrap. The last lines give the theoretical parameters computed by Tokovinin & Kiyaveva (2016) by simulation of thermal and flat eccentricity distributions and for circular orbits. The statistics of multiples (5), excluded from other samples, illustrate the influence of subsystems. They increase μ' by adding kinematic “noise” and bias the mass sum that affects calculation of μ^* . Indeed, the median μ' for multiples is larger than in other samples. Motions caused by the subsystems should also randomize γ . Unrecognized multiples remaining in the sample might bias the results to some extent, especially at large s .

Table 1 demonstrates that the statistics of relative motion in the full sample (1) are perfectly compatible with the thermal eccentricity distribution. However, the sub-samples (2) and (4) (close and wide pairs, respectively) deviate from the uniform distribution of γ in opposite ways. The difference between the γ medians between these sub-samples, $9.6^\circ \pm 2.8^\circ$, is statistically significant. Figure 4 shows the distributions of γ for close (100-250 au) and wide (1-10 kau) pairs, with a similar number of pairs in each group. Close pairs appear to be sub-thermal (less eccentric), wide pairs suggest a super-thermal eccentricity distribution. Wide pairs seem to have an excess of $\gamma < 30^\circ$ values. Interestingly, the histogram for the close binaries might contain a similar excess, while the remaining pairs have a γ distribution increasing towards $\gamma = 90^\circ$, indicative of a sub-thermal eccentricity distribution.

The parameter μ' depends on the estimated masses and is biased to larger values by undetected subsystems. On the other hand, the angle γ is a purely geometric parameter. Both the measurement errors and the additional motions caused by subsystems can only smooth the true distribution of γ . Therefore, the deviation of γ from the uniform distribution evidenced by Table 1 is a robust, albeit qualitative, indicator of the non-thermal eccentricity distribution.

When the sample is split into groups according to the mass ratio or primary mass, the resulting distributions of γ show no difference. However, when I compare 122 wide twins ($q > 0.95$) with $s > 500$ au with 213 similarly wide pairs with $0.8 < q < 0.95$, the median γ values are 36.7 ± 3.6

and 44.0 ± 3.9 degrees, respectively, suggesting that wide twins might have more eccentric orbits.

3.2 Recovering the eccentricity distribution

In this Section the eccentricity distribution $f(e)$ is inferred from the joint distribution of μ', γ using the method of Tokovinin & Kiyaveva (2016), briefly recalled here. The histogram of (μ', γ) is computed on a 15×9 grid (0.1 bin size in μ' and 10° bins in γ). Such distributions for simulated binaries with eccentricity in a narrow range, e.g. from 0 to 0.1, constitute a set of theoretical distributions (templates). Each template is evaluated for 10^4 simulated binaries. Parameters of simulated binaries such as mass sum, parallax, and separation are sampled randomly from the real data, and appropriate cuts are applied ($\rho > 2''$, $s > 100$ au, $\sigma_\gamma < 50^\circ$). This accounts for potential biases in the real sample.

The observed distribution of (μ', γ) is modeled by a linear combination of templates with 10 coefficients f_k satisfying the constraint $\sum_k f_k = 1$. Let $n_{i,j}$ be the number of binaries in the i -th and j -th bin of the histogram (i corresponds to μ' and j to γ), $T_{i,j,k}$ – the template for the k -th eccentricity bin, normalized to a unit sum over i and j . The model is $n'_{i,j} = N \sum_k T_{i,j,k} f_k$, where N is number of binaries in the sample. The goodness of fit is quantified by the parameter $\chi^2 = \sum_{i,j} (n_{i,j} - n'_{i,j})^2 / \sigma_{i,j}^2$, assuming Poisson errors $\sigma_{i,j}^2 = n_{i,j}$ and $\sigma_{i,j}^2 = 1$ if $n_{i,j} = 0$.

A small smoothing parameter α is introduced to favor continuous distributions and effectively damp the noise in the resulting f_k . The distribution f_k is found by minimizing

$$\sum_{i,j} (n_{i,j} - n'_{i,j})^2 + \alpha \sum_k (f_k - f_{k+1})^2 \rightarrow \min. \quad (2)$$

with the constraint $\sum_k f_k = 1$. A linear equation can be derived from (2), yielding the solution f_k as a simple matrix-vector product. Note that the minimization does not use weights corresponding to $\sigma_{i,j}$ for reasons explained by Tokovinin & Kiyaveva (2016), namely to reduce the influence of small $n_{i,j}$ that can be biased, e.g. by fast movers, and to give more weight to the histogram bins with large values. Therefore, the solution of (2) does not correspond to the χ^2 minimum. Compared to Tokovinin & Kiyaveva (2016), the regularization term is changed from $\alpha \sum_k f_k^2$ to the sum of squared differences. The new formulation models the data by a smooth distribution f_k , while the previous formulation biased the result towards a uniform distribution. However, the results delivered by those two alternative regularization schemes are almost identical.

Adequacy of the model is confirmed by checking that the normalized values of $\chi^2 / (135 - 9)$ are close to one (135 is the number of bins, 9 is the number of degrees of freedom). For 9 degrees of freedom, the “1 σ ” confidence limit (68.3%) corresponds to the hyper-volume in the parameter space where χ^2 increases by less than 10.4 relative to its minimum (Press et al. 2007). The regularization parameter α is increased from 10^{-3} with a step of 2 times until the χ^2 exceeds its minimum value by more than 10.4; then the previous (one step back) α is adopted. Typically, $\alpha \approx 10^{-2}$ for $N \sim 500$.

The solution of (2) does not guarantee that all $f_k \geq 0$. When a negative f_k is encountered, it is set to zero and the

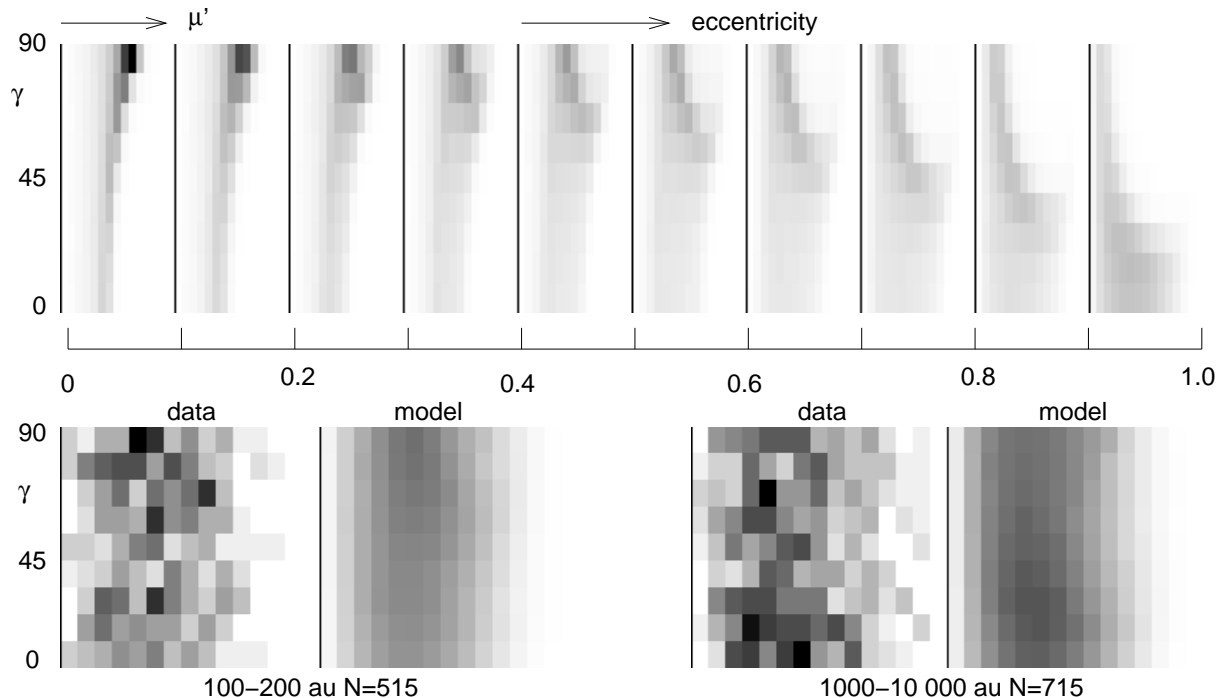


Figure 5. Restoration of the eccentricity distribution. Top row: ten templates in order of increasing eccentricity. Bottom row: observed histograms and their models.

Table 2. Eccentricity distribution

Separation	N	$\langle e \rangle$	$\chi^2/126$	f_1	f_2	f_3	f_4	f_5	f_6	f_7	f_8	f_9	f_{10}
100–10 ⁴ au	2463	0.684	1.22	0.002	0.033	0.046	0.053	0.102	0.128	0.095	0.134	0.169	0.238
100–200 au	515	0.639	1.31	0.018	0.024	0.040	0.069	0.113	0.148	0.155	0.145	0.139	0.148
100–200 au ^a	515	0.643	1.22	0.021	0.026	0.038	0.067	0.111	0.144	0.149	0.142	0.144	0.159
200–10 ³ au	1233	0.677	1.25	0.000	0.033	0.049	0.059	0.092	0.124	0.119	0.140	0.171	0.213
10 ³ –10 ⁴ au	715	0.683	1.37	0.023	0.029	0.040	0.059	0.080	0.096	0.113	0.147	0.188	0.227

^a Alternative templates generated using only binaries with $s = 100 - 200$ au are used.

fit is repeated with the reduced number of free parameters (so-called non-negative least squares).

Figure 5 illustrates the method. The upper panel shows 10 template distributions, all on the same gray scale. The vertical axis is γ , the horizontal axis is μ' ranging from 0 to 1.5 in each template. At small eccentricity, the maximum is near $\gamma = 90^\circ$, $\mu' = 1$, while small γ dominate for eccentric orbits. The lower panels show the observed distributions in two separation ranges and their models.

The method was applied to the full sample and to various cuts in separation. Representative results are given in Table 2 and plotted in Fig. 6. Columns 3 and 4 of Table 2 give the mean eccentricity $\langle e \rangle$ and the goodness of fit metric $\chi^2/126$, which is larger than one because no weights are used. At 200–10³ au separations, $f(e)$ is practically thermal. At separations below 200 au the deficit of large eccentricities becomes apparent, while at separations of 1–10 kau $f(e)$ becomes slightly super-thermal. However, undetected sub-systems mostly affect $f(e)$ at the largest separations, so the result should be taken with some caution.

At the shortest separations, the cuts applied to the data affect the statistics because the closest and fastest-moving

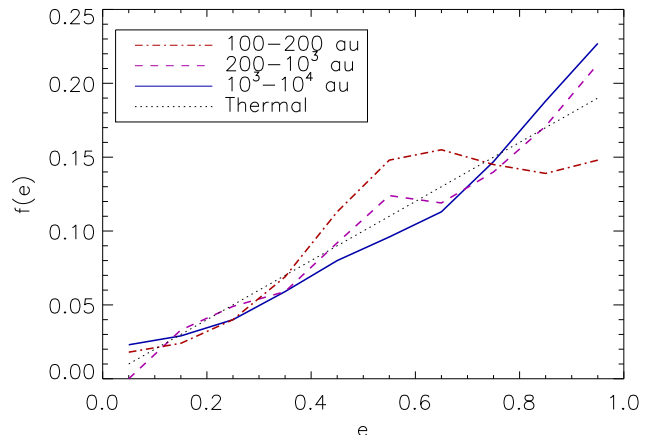


Figure 6. Eccentricity distributions.

binaries might fall below the $2''$ cutoff in ρ . The templates were re-computed by selecting only pairs with $s < 200$ au from the real sample and, indeed, they differ from the templates obtained using the full sample, although they look

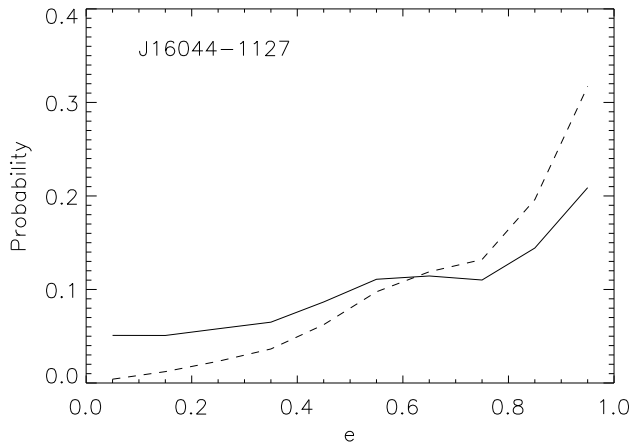


Figure 7. Posterior eccentricity distributions of ADS 9910 (WDS J16044–1127). Full line – uniform prior, dashed line – linear prior.

qualitatively similar. For the 100-200 au sample, the calculation was repeated using those more appropriate templates (see the numbers in italics in Table 2). Indeed, a lower χ^2 was obtained, but the resulting f_k differ from the standard calculation by no more than 0.01.

3.3 Posterior eccentricity distribution

In some cases, constraints on the eccentricity of a particular wide binary are useful, e.g. to find the minimum periastron separation and evaluate the influence of the wide companion on an inner subsystem or a circumstellar disk. In response to this need, sampling techniques like “Orbits for the Impatient” (OFTI) were developed to derive posterior distributions of orbital parameters from incomplete data (Blunt et al. 2017). A simpler and faster way to relate the two observables $x_0 = (\mu', \gamma)$ with the posterior eccentricity distribution is outlined here. The joint distribution of x and e can be written as

$$f(e, x) = f_1(x|e) f(e). \quad (3)$$

If $f(e)$ in the right-hand part is replaced by the prior distribution $f_0(e)$ and x takes the observed value x_0 , we obtain the posterior distribution $f(e|x_0)$. The conditional distribution $f_1(x|e)$ is obtained from simulations and is equivalent to the templates $T_{i,j,k}$ with suitable re-normalization.

To give an example, Fig. 7 plots the posterior eccentricity distributions of a typical nearby wide binary ADS 9910 ($s = 335$ au, $P^* = 4.5$ kyr) corresponding to the uniform and linear prior distributions $f_0(e)$. The observed parameters are $\mu' = 0.33$ and $\gamma = 30^\circ$, and there are no inner subsystems. Although a large eccentricity is more likely, any eccentricity is possible, hence this posterior constraint is fuzzy. However, in other instances the posterior constraints can be stronger and less dependent on the prior. For example, $\mu' \leq 1$ for circular orbits, so an observed value $\mu' > 1$ immediately excludes circular orbits. Similarly, large eccentricities can be ruled out for certain combinations of μ' and γ .

The posterior distributions of orbital parameters such as eccentricity depend on the adopted prior distributions, i.e. are model-dependent. In the sampling methods like OFTI,

the derived posterior distributions depend on the distribution of samples in the multi-dimensional space of orbital parameters. This work proves that a linear eccentricity distribution is the recommended prior for wide binaries, while a uniform prior should be deprecated in this context.

4 DISCUSSION

In § 5.1.4 of their review on multiplicity statistics, Duchêne & Kraus (2013) wrote that observations provide a “clear and uniform picture” of the eccentricity distribution, but in the same paragraph propose two different models of $f(e)$, flat and Gaussian. Their discussion refers mostly to spectroscopic binaries. Figure 15 of Raghavan et al. (2010) gives $f(e)$ for visual binaries that is approximately flat between 0.1 and 0.6 and drops at large and small e . Based on this result, some authors adopted a flat $f(e)$ between 0 and 0.8 and $f(e) = 0$ at $e > 0.8$.

Tokovinin & Kiyaveva (2016) derived $f(e)$ that rises linearly at $e < 0.8$ and remains constant at larger e . The median separation in their sample was 120 au. This result is confirmed here using a different, larger sample (red curve in Fig. 6). They also demonstrated a good agreement between the reconstructed eccentricity distribution and $f(e)$ derived from known visual orbits with $P > 100$ yr, except for the last bin lacking eccentric orbits. The paucity of binaries with $e > 0.8$ in the sample of Raghavan et al. (2010) is explained by the bias in the orbit catalogue, while in fact such pairs are frequent.

At separations $s > 200$ au, the eccentricity distribution becomes consistent with the thermal one. Moreover, this study shows that pairs with $s > 1$ kau might have a slightly super-thermal eccentricity distribution. The $f(e)$ derived here for these binaries could potentially be biased by undiscovered subsystems. However, the statistics of γ , less affected by subsystems, also suggest a super-thermal eccentricity distribution at $s > 1$ kau. It is possible that the trend to super-thermal $f(e)$ at large separations is even stronger than found here.

A close match of the observed eccentricity distribution to the thermal distribution suggests that dynamical processes played an important role in the formation of wide binaries. For example, pairs that remain after dynamical interaction of a binary or a triple system with another star (scattering) have a nearly thermal $f(e)$ (e.g. Fig. 16 in Antognini & Thompson 2016). When two binaries interact dynamically in a gas cloud and survive as a 2+2 quadruple, the eccentricity of the wider remaining pair has a super-thermal distribution, while for the closer pair the distribution is thermal (Fig. 9 of Ryu et al. 2017). Disintegration of unstable triple systems leaves binaries with a mildly super-thermal $f(e)$ (Stone & Leigh 2019). However, wide binaries formed by ejection from unstable triples or “unfolding” (Reipurth & Mikkola 2012) must have only very eccentric orbits. The unfolding mechanism does not match certain properties of real wide binaries and appears to be exceptional rather than typical (Tokovinin 2017).

Hydrodynamical simulations show that protostars formed at large distances from each other can get bound into a wide pair with the help of gas friction (Bate 2019; Kuffmeier et al. 2019). Continued accretion onto such bi-

nary shortens its period and reduces the eccentricity. From this perspective, eccentric orbits are produced naturally even without dynamical interactions with other stars; a positive correlation between separation and eccentricity is expected. This formation channel of wide binaries works even in low-density environments. However, no predictions of the resulting eccentricity distribution are available so far. Simulations of a dense cluster by Bate (2019) inform us on the binary statistics, but in this environment dynamical interactions between stars are important and the resultant statistics reflect a complex interplay of several processes.

To disentangle the relative roles of stellar dynamics and gas-assisted capture in the formation of wide binaries, it will be interesting to apply this method to sparse associations like Taurus-Auriga and to moving groups. Small sample size and the need to account for the subsystems present obvious challenges to this endeavor.

ACKNOWLEDGMENTS

I thank Karim El-Badry and Maxwell Moe for comments on the early version of this work and the anonymous Referee for helping to improve the presentation. This study used the Washington Double Star Catalogue maintained at USNO. It has made use of data from the European Space Agency (ESA) mission *Gaia* (<https://www.cosmos.esa.int/gaia>), processed by the *Gaia* Data Processing and Analysis Consortium (DPAC, <https://www.cosmos.esa.int/web/gaia/dpac/consortium>). Funding for the DPAC has been provided by national institutions, in particular the institutions participating in the *Gaia* Multilateral Agreement.

REFERENCES

- Antognini, J. M. O. & Thompson, T. A. 2016, MNRAS, 456, 4219
- Bate, M. R. 2019, MNRAS, 484, 2341.
- Belokurov, V., Penoyre, Z., Oh, S., et al. 2020, preprint arxiv:200305467
- Blunt, S., Nielsen, E. L., De Rosa, R. J., et al. 2017, AJ, 153, 229
- Brandt, T. D. 2018, ApJS, 239, 31
- Bressan, A., Marigo, P., Girardi, L., et al. 2012, MNRAS, 427, 127
- Duchêne, G. & Kraus, A. 2013, ARAA, 51, 269
- El-Badry, K. & Rix, H.-W. 2018, MNRAS, 480, 488 (ER2018)
- El-Badry, K., Rix, H.-W., Tian, H., et al. 2019, MNRAS, 489, 5822
- Gaia Collaboration, Brown, A. G. A., Vallenari, A., Prusti, T., et al. 2018, A&A, 595A, 2 (Vizier Catalogue I/345/gaia2).
- Geller, A. M., Leigh, N. W. C., Giersz, M., et al. 2019, ApJ, 872, 165
- Kuffmeier, M., Calcutt, H., & Kirstensen, L. E. 2019, A&A, 628, 112
- Mason, B. D., Wycoff, G. L., Hartkopf, W. I., Douglass, G. G. & Worley, C. E. 2001, AJ, 122, 3466 (WDS)
- Pittordis, C. & Sutherland, W. 2019, MNRAS, 488, 4740
- Press, W. H., Teukolsky, S. A., Vetterling, T., & Flannery, B. P. Numerical Recipes, The Art of Scientific Computing. 2007, Cambridge Univ. Press, Cambridge
- Raghavan, D., McAlister, H. A., Henry, T. J., et al. 2010, ApJS, 190, 1
- Reipurth, B. & Mikkola, S. 2012, Nature, 492, 221
- Ryu, T., Leigh, N. W. C., & Perna, R. 2017, MNRAS, 467, 4447
- Stone, N. C. & Leigh, N. W. C. 2019, Nature, 576, 406
- Tokovinin, A. & Kiyaveva, O. 2016, MNRAS, 456, 2070
- Tokovinin, A. 2017, MNRAS, 468, 3461
- Tokovinin, A. 2018, ApJS, 235, 6

5 SUPPLEMENTARY MATERIAL

The supplementary file lists μ , γ , μ^* , and other parameters described in the text for 3601 wide pairs from the ER2018 catalogue located within 67 pc.